Int. J. Heat Mass Transfer. Vol. 17, pp. 1425–1436. Pergamon Press 1974. Printed in Great Britain

MASS TRANSPORT AROUND TWO SPHERES AT LOW REYNOLDS NUMBERS

KARAMAT AMINZADEH, T. R. AL TAHA and A. R. H. CORNISH
Imperial College of Science and Technology, London, England

and

M. S. KOLANSKY and ROBERT PFEFFER
The City College of New York, New York, New York, U.S.A.

(*Received* 18 *September* 1973 *and in revised form* 14 *January* 1974)

Abstract—A relaxation technique has been used to solve the conservation of species equation to obtain mass-transfer rates around two equally sized spheres placed parallel to their line of centers in Stokes' flow. Four different sphere spacings were studied in the Peclét number range of 0–50. It was found that the overall Sherwood number for either sphere was always less than that of a single isolated sphere, and at low Peclét numbers, overall Sherwood numbers of less than 2 were obtained.

NOMENCLATURE

a, characteristic dimension in bipolar coordinates defined by Fig. 2;
a^*, a/R;
C^*, dimensionless concentration, $(C-C_o)/(C_s-C_o)$;
C_o, concentration at ∞;
C_s, concentration at surface of spheres;
d, characteristic dimension in bipolar coordinate defined by Fig. 2;
$\mathscr{D}$, diffusivity;
h, step size in z direction;
k, step size in θ direction;
L, center-to-center distance between the two spheres;
$mm1$, number of steps in the z direction;
$m1$, number of steps in the σ direction;
m, $m1-1$;
n, numerical index;
N_{Re}, Reynolds number, $2RU_\infty/\nu$;
N_{Pe}, Peclét number, $2RU_\infty/\mathscr{D}$;
$N_{Sh_{O_A}}$, overall Sherwood number around sphere A;
$N_{Sh_{O_B}}$, overall Sherwood number around sphere B;
$N_{Sh_{L_A}}$, local Sherwood number, sphere A;
$N_{Sh_{L_B}}$, local Sherwood number, sphere B;
P, pressure;
P_n, Legendre polynomial;
R, sphere radius;
r, outer boundary defined by Fig. 2;
R_∞, dimensionless outer boundary, r/d;
U_∞, free stream velocity;
$\mathbf{V}$, fluid velocity vector;
V_θ, fluid velocity component in the θ direction;
V_z, fluid velocity component in the z direction;
V_θ^*, dimensionless velocity, V_θ/U_∞;
V_z^*, dimensionless velocity, V_z/U_∞;
z, bipolar coordinate.

Greek symbols

α, surface of sphere, $|z_s|$;
μ, fluid viscosity;
ν, fluid kinematic viscosity;
θ, bipolar coordinate;
ψ, stream function.

INTRODUCTION

MASS or heat transfer involving particles at very low Reynolds numbers are important in such diverse fields as combustion of finely dispersed fuels, spray drying, meteorological studies, ion exchange, and gas chromatography. It is well known that the minimum possible rate of mass (or heat) transfer from a single sphere contained within an infinite stagnant fluid corresponds to a Sherwood (or Nusselt) number of two and that the Sherwood number increases with the relative velocity between the fluid and the solid [1–3] and with a decrease in the voidage in the multiparticle system [4], [5]. Frequently, however, in multiparticle systems such as fluidized beds, values of the Nusselt number less than two have been measured. A variety of reasons—such as backmixing—have been put forward to explain this apparent inconsistency. It does not seem to have been generally accepted that, for multiparticle systems, the

minimum theoretical value of the Sherwood (or Nusselt) number can, under certain conditions, be less than two even though the reasoning behind this argument has been fully documented by Cornish [6].

In this study the rate of mass transfer around two identical active spheres with their line of centers parallel to the main direction of flow in "creeping motion" has been determined by solving the diffusion equation numerically. The results clearly show the important hydrodynamic effect of particle-to-particle interaction on both the local and overall mass-transfer rates from each of the two spheres. In the limit of zero Reynolds number overall Sherwood numbers of less than two are obtained for all sphere spacings considered and Sherwood numbers less than two were also obtained for finite Reynolds numbers depending on the sphere spacing. It is hoped that these results for the flow around the simple configuration of two identical spheres will lend some insight into the complex behavior of the mass transfer process in multiparticle systems such as packed and fluidized beds.

THEORETICAL ANALYSIS

Consider the creeping flow ($N_{Re} \ll 1$) of a Newtonian, incompressible fluid past two equally sized spheres of radius R parallel to their line of centers as shown in Fig. 1. We assume that the spheres are partially soluble

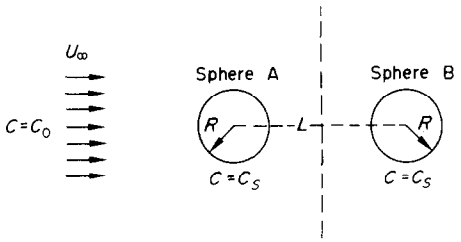

FIG. 1. Flow configuration.

in the fluid flowing past them so that mass transfer between the spheres and the fluid occurs. However, we further assume that the solubility is so small that the change in size of the spheres during a finite time period is negligible. For steady state conditions the continuity, creeping motion, and conservation of species equations are:

$$\nabla . \mathbf{V} = 0 \tag{1}$$

$$\nabla P = \mu \nabla^2 \mathbf{V} \tag{2}$$

$$\mathbf{V} . \nabla C = \mathscr{D} \nabla^2 C. \tag{3}$$

Equations (1) and (2) have already been solved by Stimson and Jeffrey [7] in bipolar coordinates z, θ (see Fig. 2) for the case of two equal sized spheres falling parallel to their line of centers in an incompressible viscous fluid. The solution in terms of the Stokes stream function is given as:

$$\psi(z, \theta) = (\cosh z - \cos\theta)^{-3/2} \sum_{n=1} U_n(z) V_n(\theta) \tag{4}$$

where

$$U_n(z) = A_n \cosh(n-\tfrac{1}{2})z + B_n \cosh(n+\tfrac{3}{2})z \tag{5}$$

$$A_n = -(2n+3)K \times \left[\frac{2(1-e^{-(2n+1)\alpha})+(2n+1)(e^{2\alpha}-1)}{2\sinh(2n+1)\alpha+(2n+1)\sinh 2\alpha}\right] \tag{6}$$

$$B_n = (2n-1)K \times \left[\frac{2(1-e^{-(2n+1)\alpha})+(2n+1)(1-e^{-2\alpha})}{2\sinh(2n+1)\alpha+(2n+1)\sinh 2\alpha}\right] \tag{7}$$

$$K = \frac{a^2 U_\infty (n+1)n}{\sqrt{2}(2n-1)(2n+1)(2n+3)} \tag{8}$$

$$\alpha = |z_s|, \quad \text{surface of the sphere} \tag{9}$$

$$V_n(\theta) = P_{n-1}(\cos\theta) - P_{n+1}(\cos\theta); \quad P = \text{Legendre function.} \tag{10}$$

Since we require a solution for the case of two fixed spheres with the fluid streaming past them with a constant velocity U_∞, equation (4) can be readily transformed to our requirements by noting that in the undisturbed bulk flow:

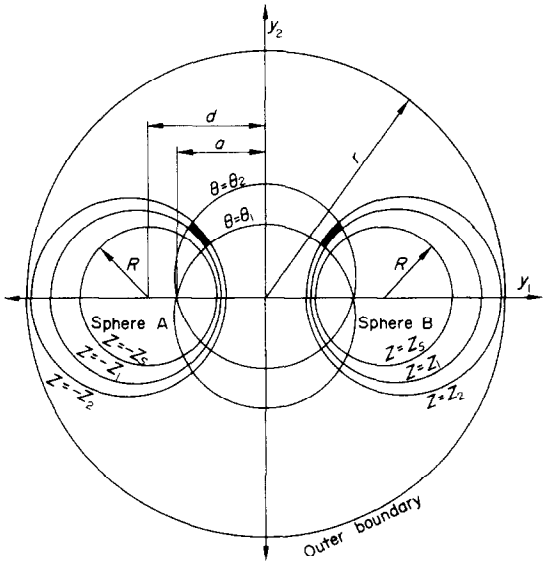

FIG. 2. Bipolar coordinates; z, θ.

$$\psi = \tfrac{1}{2} U_\infty y_2^2 \tag{11}$$

where y_2 is the distance measured along the perpendicular to the axis of symmetry (see Fig. 2).

Equation (11) when converted into bipolar coordinates yields:

$$\psi(z,\theta)=\tfrac{1}{2}\frac{a^2\sin^2\theta U_\infty}{(\cosh z-\cos\theta)^2}. \tag{12}$$

By adding equations (4) and (12) we obtain the stream function for the flow past the spheres

$$\psi(z,\theta)=\frac{\tfrac{1}{2}a^2\sin^2\theta U_\infty}{(\cosh z-\cos\theta)^2}+(\cosh z-\cos\theta)^{-3/2}\sum_{n=1}U_n(z)V_n(\theta). \tag{13}$$

The velocity components V_z and V_θ as a function of the stream function are given as:

$$V_z=-\frac{(\cosh z-\cos\theta)^2}{a^2\sin\theta}\frac{\partial\psi}{\partial\theta} \tag{14a}$$

$$V_\theta=\frac{(\cosh z-\cos\theta)^2}{a^2\sin\theta}\frac{\partial\psi}{\partial z}. \tag{14b}$$

In terms of the dimensionless velocities $V_z^*=V_z/U_\infty$ and $V_\theta^*=V_\theta/U_\infty$ the final expressions for the velocity in the z and θ directions are:

$$\begin{aligned}V_z^*=&\frac{1-\cos\theta\cosh z}{\cosh z-\cos\theta}+\tfrac{3}{2}(\cosh z-\cos\theta)^{-1/2}\\&\times\sum_n\left[A_n^*\cosh(n-\tfrac{1}{2})z+B_n^*\cosh(n+\tfrac{3}{2})z\right]\\&\times\left[P_{n-1}(\cos\theta)-P_{n+1}(\cos\theta)\right]-\frac{(\cosh z-\cos\theta)^{1/2}}{\sin\theta}\\&\times\sum_n\left[A_n^*\cosh(n-\tfrac{1}{2})z+B_n^*\cosh(n+\tfrac{3}{2})z\right]\\&\times\left[\frac{1}{\sin\theta}\left[n\{P_n(\cos\theta)-\cos\theta P_{n-1}(\cos\theta)\}\right.\right.\\&\left.\left.+(n+2)\{\cos\theta P_{n+1}(\cos\theta)-P_{n+2}(\cos\theta)\}\right]\right]\end{aligned} \tag{15}$$

$$\begin{aligned}V_\theta^*=&\frac{-\sin\theta\sinh z}{\cosh z-\cos\theta}-\tfrac{3}{2}\frac{\sinh z}{\sin\theta}(\cosh z-\cos\theta)^{-1/2}\\&\times\sum_n\left[A_n^*\cosh(n-\tfrac{1}{2})z+B_n^*\cosh(n+\tfrac{3}{2})z\right]\\&\times\left[P_{n-1}(\cos\theta)-P_{n+1}(\cos\theta)\right]+\frac{(\cosh z-\cos\theta)^{1/2}}{\sin\theta}\\&\times\sum_n\left[A_n^*(n-\tfrac{1}{2})\sinh(n-\tfrac{1}{2})z+B_n^*(n+\tfrac{3}{2})\right.\\&\left.\times(\sinh(n+\tfrac{3}{2})z)\right].\left[P_{n-1}(\cos\theta)-P_{n+1}(\cos\theta)\right]\end{aligned} \tag{16}$$

where

$$A_n^*=-(2n+3)K^*\left(2(1-e^{-(2n+1)\alpha})+(2n+1)(e^{2\alpha}-1)\right) \tag{17a}$$

$$B_n^*=(2n-1)K^*\left(2(1-e^{-(2n+1)\alpha})+(2n+1)(1-e^{-2\alpha})\right) \tag{17b}$$

$$K^*=\frac{n(n+1)}{\sqrt{2(2n-1)(2n+1)(2n+3)(2\sinh(2n+1)\alpha+(2n+1)\sinh 2\alpha)}}. \tag{17c}$$

These values for the velocity distribution can then be used in equation (3) to solve for the concentration distribution around the spheres.

In terms of the dimensionless variables V_z^*, V_θ^*, $C^*=C-C_0/C_s-C_0$, $a^*=a/R$, and $N_{Pe}=2RU_\infty/\mathscr{D}$ and changing to bipolar coordinates, equation (3) becomes for axisymmetric flow:

$$\frac{\partial}{\partial z}\left(\frac{\sin\theta}{\cosh z-\cos\theta}\frac{\partial C^*}{\partial z}\right)+\frac{\partial}{\partial\theta}\left(\frac{\sin\theta}{\cosh z-\cos\theta}\frac{\partial C^*}{\partial\theta}\right)=\frac{\tfrac{1}{2}N_{Pe}a^*\sin\theta}{(\cosh z-\cos\theta)^2}\left(V_z^*\frac{\partial C^*}{\partial z}+V_\theta^*\frac{\partial C^*}{\partial\theta}\right). \tag{18}$$

Equation (18) must be solved subject to the boundary conditions:

(i) at the surface of each sphere the solute concentration remains constant, i.e. at $z=\pm z_s$, $C^*=1$,

(ii) along the axis of symmetry the concentration gradient is zero, i.e. at $\theta=0$ and $\theta=\pi$, $\partial C^*/\partial\theta=0$,

(iii) very far from the two spheres, the dimensionless solute concentration is zero, i.e. at $r=\infty$, $C^*=0$.

FINITE DIFFERENCE APPROXIMATIONS

The first step in any numerical method is to replace the differential equation by its finite difference approximation. Figure 3 shows the bipolar coordinate system transformed into a rectangular lattice of mesh length h in the z direction and k in the θ direction. An approximate solution of the conservation of species equation (18) will be obtained at a finite number of grid points having coordinates $z=ih$, $\theta=jk$ where i and j are integers, with i going from 1 to $mm1$ and j from 1 to $m1$.

Equation (18) written in finite difference form (see Appendix for the detailed development of the finite difference approximations) becomes:

$$C_{i,j}^*=B_1(i,j)C_{i+1,j}^*+B_2(i,j)C_{i-1,j}^*+B_3(i,j)C_{i,j+1}^*+B_4(i,j)C_{i,j-1}^* \tag{19}$$

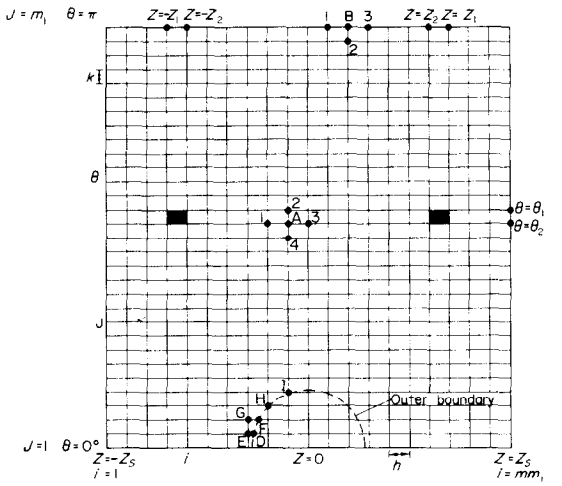

FIG. 3. Rectangular mesh; z, θ.

where B_1, B_2, B_3 and B_4 are coefficients defined in the appendix.

A numerical solution of equation (19) using relaxation at all mesh points of the field can be obtained when the appropriate boundary conditions are specified everywhere on the boundary. However, as shown in the appendix, special treatment is required in using the boundary conditions at the axis of symmetry and very far from the spheres ($r \approx \infty$). Along the axis of symmetry ($\theta = 0$ and $\theta = \pi$) the following two equations apply:

For $\theta = 0$

$$C^*_{i,1} = A_1(i)C^*_{i+1,1} + A_2(i)C^*_{i-1,1} + A_3 C^*_{i,2}. \quad (20)$$

For $\theta = \pi$

$$C^*_{i,m1} = D_1(i)C^*_{i+1,m1} + D_2(i)C^*_{i-1,m1} + D_3 C^*_{i,m}. \quad (21)$$

The coefficients A_i and D_i are also defined in the appendix.

Very far from the two spheres we require that the dimensionless concentration C^* be set equal to zero. For numerical purposes we assume that the concentration is equal to zero in the region outside of a spherical boundary of dimensionless radius $R_\infty = r/d$. The outer boundary which encloses the two spheres when transformed into bipolar coordinates is represented by the equation:

$$\cosh(z) = \frac{((r/d)^2/\tanh^2 z_s)+1}{((r/d)^2/\tanh^2 z_s)-1}\cos(\theta). \quad (22)$$

Figure 2 defines the values of r and d and the dotted line curve in Fig. 3 represents the outer boundary in the $z-\theta$ plane. The area enclosed by the curve represents a dimensionless concentration of zero. The solution of equation (22) obviously yields points that do not fall exactly on one of the equally spaced mesh points. When this occurred the concentration was set equal to zero at the next larger absolute value of z. This is illustrated in Fig. 3. The boundary equation (22) gives points D, F, H and I. Points D and F do not lie at a mesh point and, therefore, points E and G are substituted for points D and F, respectively and the concentration set equal to zero at these points instead.

The application of the boundary conditions at the surface of each sphere, i.e. at $z = -z_s$, $C^*_{1,j} = 1$ and at $z = +z_s$, $C^*_{mm1,j} = 1$ did not lead to any added difficulty. Using the five boundary conditions, the finite difference equations were solved iteratively by the extrapolated method of Gauss–Seidel. A different relaxation factor Ω was chosen by trial and error for each sphere spacing and Peclét number considered so as to give a stable and converging solution. The relaxation factor used varied between 1·8 and 0·034 with large relaxation factors required at low Peclét numbers and small relaxation factors required at high Peclét numbers. Using a mesh spacing of 3 degrees or 61 points in the θ direction and 41 or 43 points (depending on the sphere spacing) in the z direction, the $z-\theta$ lattice consisted of roughly 2500 mesh points. The solution was assumed to have converged when the concentrations at all but ten of the mesh points were within a specified tolerance between two successive iterations. The choice of ten unconverged points was assumed arbitrarily. More complete details of the numerical procedures and a listing of the computer programs used can be found in reference [9].

DISCUSSION OF RESULTS

Numerical solutions of the conservation of species equation were obtained for four different sphere spacings and Peclét numbers in the range of 0–50. It was found that the quality of the solutions depended on (a) the number of terms used in the Stimson and Jeffrey velocity profile, (b) the value of R_∞ chosen for the outer boundary, and (c) the value of the tolerance specified between two successive iterations.

Initially the computer program was written to use a fixed number of velocity terms. It was found, however, that the solutions changed depending upon the number of terms used. A study was conducted as to how many velocity terms were needed before the solutions ceased to vary. These values are given for each of the sphere spacings studied in the table below.

Sphere spacing z_s	L/R	*Number of terms*
0·2	2·0402	35
1·0	3·0862	8
2·1	8·228	5
3·0	20·140	4

In order to generalize the final program a routine was added that automatically determines the correct number of velocity terms needed for different sphere spacings.

The value of the outer boundary should, of course, be chosen as large as possible since theoretically the concentration C^* is specified as zero only at $R_\infty = \infty$. However, as the outer boundary was increased the solution required many more iterations and it became virtually impossible to achieve convergence at the higher Peclét numbers. The rate of convergence for a specified outer boundary was dependent on the sphere spacing and decreased as the sphere spacing was increased. Fortunately, however, it was found that at high Peclét numbers and large sphere spacing the choice of the outer boundary had a much smaller effect on the accuracy of the solution. Thus we were able to obtain convergence and accurate results as well in the entire Peclét number range by using smaller values of R_∞ as the Peclét number and sphere spacing were increased. For example, at a sphere spacing of $z_s = 0{\cdot}2$ we found that changing the outer boundary from $R_\infty = 14$ to $R_\infty = 7$ had a negligible effect on the numerical value of the overall Sherwood number for Peclét numbers greater than 1; at a Peclét number of 0·1, however, a value of $R_\infty = 40$ had to be used to obtain accurate results. At the large sphere spacing of $z_s = 3{\cdot}0$ we found that the outer boundary given by $R_\infty = 7$ gave acceptably accurate results in the entire Peclét number range.

The tolerance specified between two successive iterations to achieve convergence was originally set at 10^{-4}, in order to save computer time. However, we found that plots of the overall Sherwood number versus Peclét number were not smooth but tended to oscillate somewhat, especially at small sphere spacing. A tolerance of 10^{-5} gave smooth curves for all of the sphere spacing studied and the solutions were in close agreement with a selected few obtained using a tolerance of 10^{-6}. Therefore, a tolerance of 10^{-5} was used for all of the results reported below.

Local Sherwood numbers

Local values of the Sherwood number around each sphere of the two sphere system are closely related to the concentration profiles around the spheres. These profiles vary with Peclét number and the center-to-center distance between the spheres. The local Sherwood numbers for each sphere depend directly on the concentration gradient at the sphere surface and were calculated using:

$$N_{Sh_{L_A}}(\theta) = \frac{-2(\cosh(-z_s) - \cos\theta)}{a^*}\left(\frac{\partial C^*}{\partial z}\right)_{z=-z_s} \tag{23a}$$

$$N_{Sh_{L_B}}(\theta) = \frac{-2(\cosh(z_s) - \cos\theta)}{a^*}\left(\frac{\partial C^*}{\partial z}\right)_{z=z_s}. \tag{23b}$$

The local Sherwood numbers obtained from equations (23a) and (23b) were plotted vs the angle from the forward stagnation point of each sphere with Peclét number as a parameter and are shown in Figs. 4–7(a) and (b).

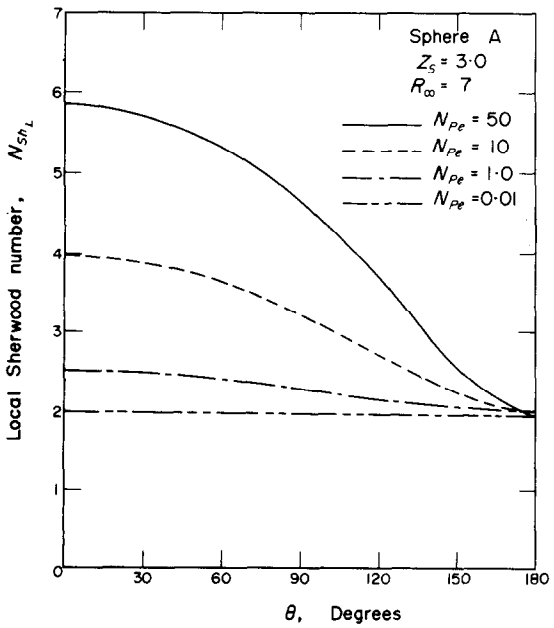

FIG. 4(a). Local Sherwood number as a function of angle θ with Peclét number as a parameter.

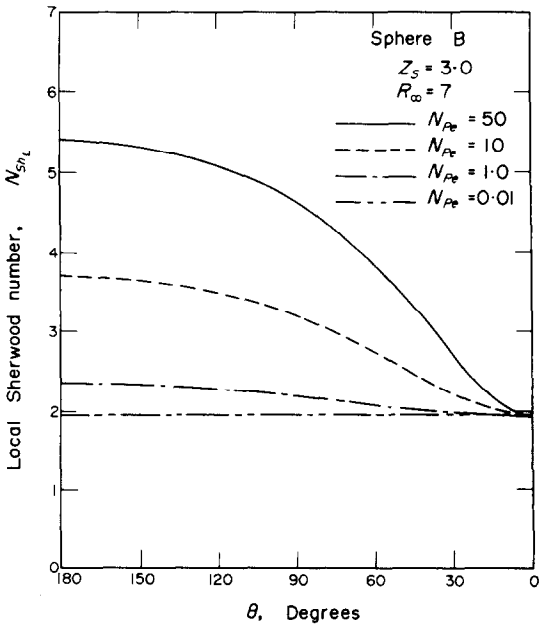

FIG. 4(b). Local Sherwood number as a function of angle θ with Peclét number as a parameter.

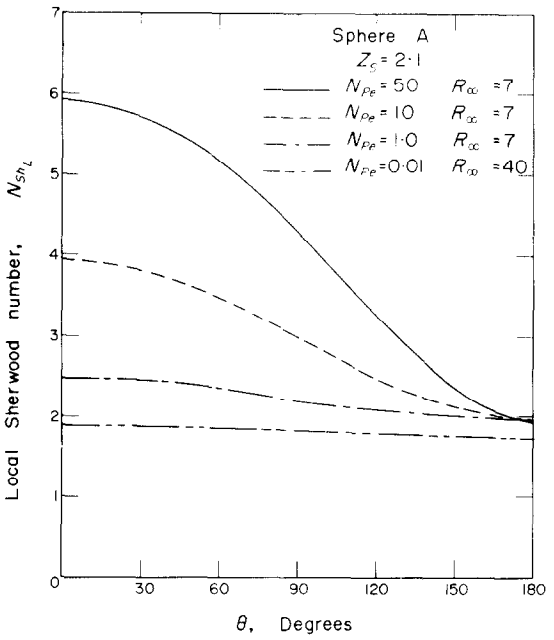

FIG. 5(a). Local Sherwood number as a function of angle θ with Peclét number as a parameter.

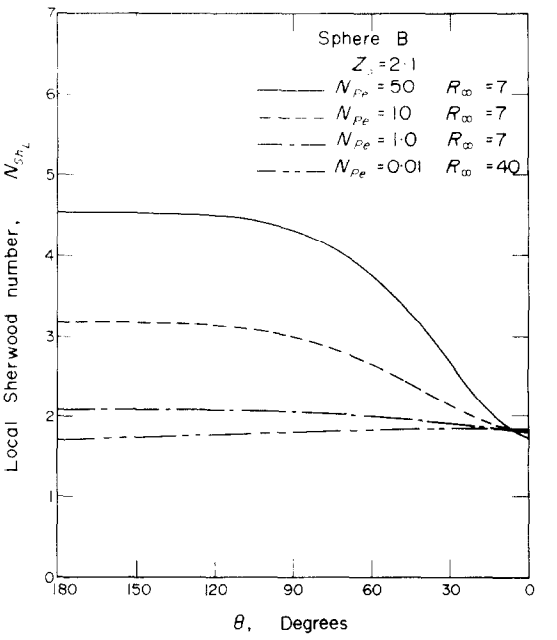

FIG. 5(b). Local Sherwood number as a function of angle θ with Peclét number as a parameter.

For $z_s = 3{\cdot}0$, $L/R = 20{\cdot}14$ the largest sphere spacing studied, Figs. 4(a) and (b) show that the higher the Peclét number the higher the mass transfer rate especially around the front of the sphere. This is due to the decrease in thickness of the diffusional boundary layer as the Peclét number increases. Because the two spheres are very far apart the curves for each sphere are very similar and resemble the curve for a single isolated sphere showing a maximum Sherwood number at the forward stagnation point, a continuous decrease around the sphere, and a minimum Sherwood number at the rear stagnation point [10]. However, the magnitude of the local Sherwood numbers, especially at the higher Peclét numbers, are somewhat lower for

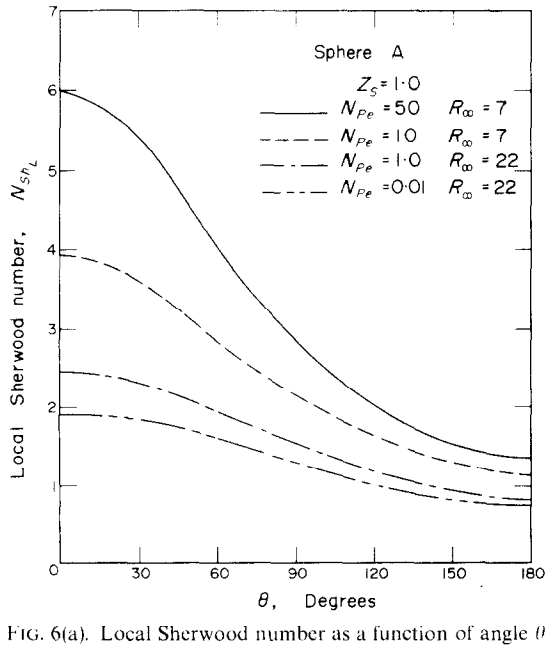

FIG. 6(a). Local Sherwood number as a function of angle θ with Peclét number as a parameter.

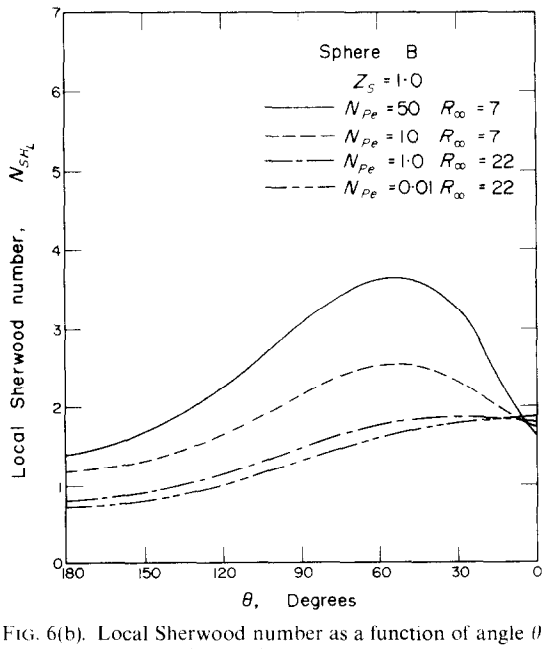

FIG. 6(b). Local Sherwood number as a function of angle θ with Peclét number as a parameter.

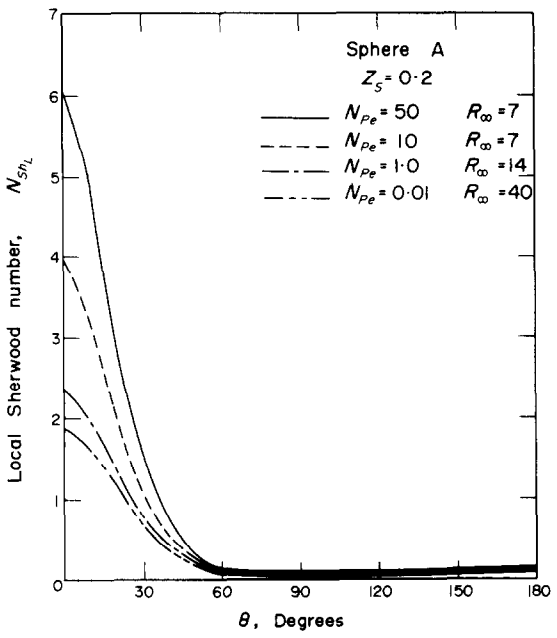

FIG. 7(a). Local Sherwood number as a function of angle θ with Peclét number as a parameter.

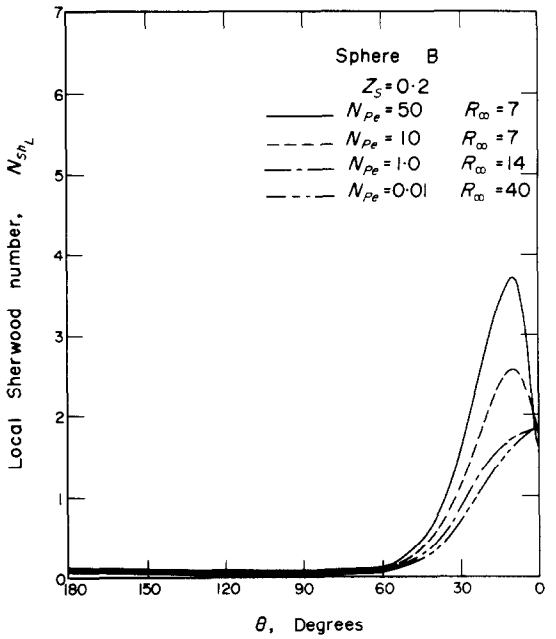

FIG. 7(b). Local Sherwood number as a function of angle θ with Peclét number as a parameter.

sphere B than for sphere A. This is because sphere A is in contact upstream with fresh fluid and thus more mass transfer takes place than downstream around sphere B. At a Peclét number of 0·01 the two spheres show almost identical behavior and the local Sherwood number remains approximately constant at 2 indicating molecular diffusion as the sole mechanism of mass transfer.

For $z_s = 2{\cdot}1$, $L/R = 8{\cdot}288$ the local Sherwood number curves (Figs. 5(a) and (b)) show similar trends as described for $z_s = 3{\cdot}0$. For sphere A the local Sherwood numbers at the forward stagnation point for each Peclét number are almost identical for the two different sphere spacings although the Sherwood numbers fall off at a faster rate for the smaller spacing. For sphere B, however, the values of the Sherwood number at the forward stagnation point are appreciably lower at the smaller spacing but fall off much slower around the sphere so that they are almost the same as for the larger spacing at the rear stagnation point. These effects are due to the greater influence of the two spheres upon one another at the smaller spacing.

Decreasing the sphere spacing even further to $z_s = 1{\cdot}0$, $L/R = 3{\cdot}0862$ results in the curves shown in Figs. 6(a) and (b). For sphere A the Sherwood numbers at the forward stagnation point continue to remain about the same as for the previous spacings but fall off very sharply around the sphere. For sphere B the behavior is quite different. At the large Peclét numbers ($N_{Pe} = 10$ and 50) the Sherwood numbers are very low at the forward stagnation point, rise to a maximum at about 130° ($\theta = 50°$), and then fall off again as the rear stagnation point is reached. At the very low Peclét number of 0·01, no maximum is observed and the Sherwood number rises continuously around the sphere. These effects are due to the close spacing between the spheres which causes the region between the two spheres to become very highly concentrated in solute so that very little mass transfer from the spheres can take place in this region.

The curves for the smallest spacing studied, $z_s = 0{\cdot}2$, $L/R = 2{\cdot}0402$ are shown in Figs. 7(a) and (b). Here the spheres are almost touching and the results are affected accordingly. For sphere A the Sherwood number curves fall off very rapidly around the sphere and the mass-transfer rate decreases to almost nil at angles of about 70° and greater. For sphere B there is negligible mass transfer around the front of the sphere, the Sherwood numbers start to rise at an angle of about 110° ($\theta = 70°$), and at Peclét numbers of 10 and 50 reach a maximum and then fall again as the rear stagnation point is reached. The curves for the very low Peclét numbers of 0·01 and 1·0 showed no maximum but continue to rise until the rear stagnation point was reached. The reason that most of the area around the back of sphere A and the front of sphere B did not contribute to mass transfer is because of the closeness of the two spheres which resulted in saturating the relatively stagnant fluid between the two spheres and dropping the driving force for mass transfer to zero. Thus the two spheres behave like a single combined body in the flowing fluid. This was clearly illustrated

by the numerical values of the concentration profile contours obtained at this spacing.

Overall Sherwood numbers

The overall Sherwood numbers for each sphere is simply the local Sherwood number integrated over the surface area of the sphere and are computed from

$$N_{Sh_{O_A}} = \frac{(\cosh z_s - 1)(\cosh z_s + 1)}{a^*} \times \int_0^{\pi} \left.\frac{\partial C^*}{\partial z}\right|_{z=-z_s} \frac{\sin\theta}{\cosh z_s - \cos\theta} \mathrm{d}\theta \quad (36a)$$

$$N_{Sh_{O_B}} = \frac{-(\cosh z_s - 1)(\cosh z_s + 1)}{a^*} \times \int_0^{\pi} \left.\frac{\partial C^*}{\partial z}\right|_{z=z_s} \frac{\sin\theta}{\cosh z_s - \cos\theta} \mathrm{d}\theta \quad (36b)$$

and plotted against Peclét number in Figs. 8–11. Smooth curves were obtained by using large values of the outer boundary R_∞ at low Peclét numbers and decreasing the outer boundary at high Peclét numbers to conserve computer time. For each spacing studied the overall Sherwood numbers for each sphere were approximately equal and constant at low Peclét numbers ($N_{Pe} < 0{\cdot}1$) where mass transfer was primarily due to molecular diffusion. At higher Peclét numbers where convection becomes important the overall mass-transfer rate was always greater around sphere A since sphere A being upstream of the flow was supplied with fresher fluid than sphere B.

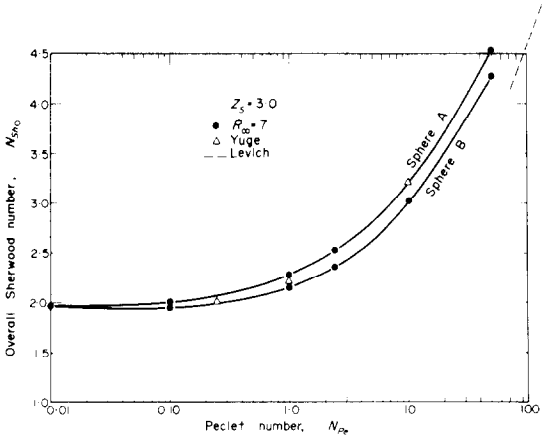

FIG. 8. Overall Sherwood number as a function of Peclét number.

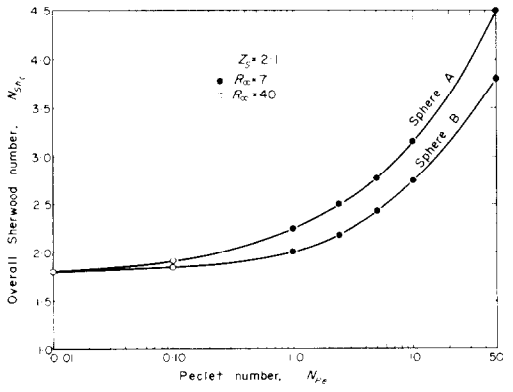

FIG. 9. Overall Sherwood number as a function of Peclét number.

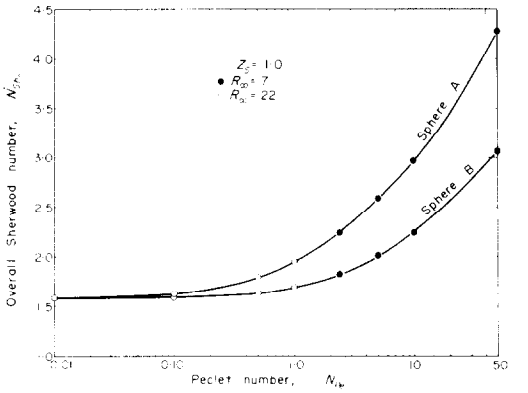

FIG. 10. Overall Sherwood number as a function of Peclét number.

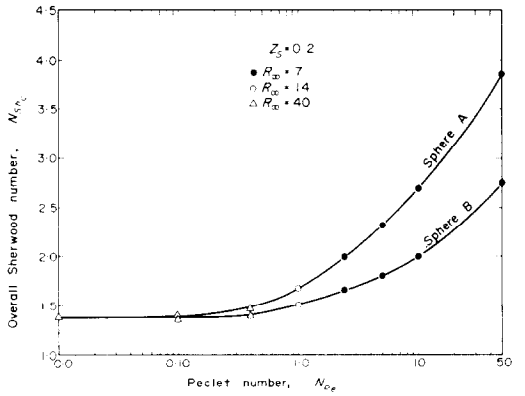

FIG. 11. Overall Sherwood number as a function of Peclét number.

For the largest sphere spacing studied, $z_s = 3{\cdot}0$ the curves for each of the two spheres (Fig. 8) are fairly close together indicating a relatively small effect of particle interaction on the mass-transfer process. Because of the large spacing between the spheres, we have included for comparison in Fig. 8 some values computed by Yuge [11] for mass transfer around a single sphere in the Peclét number range of 0·3–10 as well as the asymptotic solution for very high Peclét numbers obtained by Levich [1]. The agreement with Yuge's values are very good and the curve for sphere A also appears to approach the Levich asymptotic solution at high Peclét numbers indicating the small effect of particle interaction on the overall mass-transfer rate at this large sphere spacing.

As the spacing between the spheres is decreased the overall Sherwood numbers for both spheres A and B also decrease at any fixed Peclét number showing the increasing effects of particle interaction on the rate of mass transfer. Since the results for the largest sphere spacing $L/R = 20{\cdot}14$ are indicative of mass transfer around a single isolated sphere a comparison of Figs. 8–11 show that in Stokes flow the overall mass-transfer coefficient around either sphere in a two sphere system is always smaller than that around a single isolated sphere. These results have been qualitatively confirmed by Peltzman and Pfeffer [12] and Chen and Pfeffer [13] using an experimental two sphere system consisting of one active (benzoic acid) sphere and one inert (plastic) sphere placed either in front or behind the active sphere in a water tunnel. Although these experiments were conducted in a Reynolds number range of 8–50 and at very large Peclét numbers so that the results are not directly comparable with this study, they did indicate that the overall Sherwood number around the active sphere in the two sphere system was always less than the value for a single active sphere and always decreased as the sphere spacing was decreased.

At a spacing of $z_s = 2{\cdot}1$ and a Peclét number of $0{\cdot}1$ the overall Sherwood number is below the single sphere limiting value of 2 for both spheres A and B and at the even closer spacings of $z_s = 1{\cdot}0$ and $z_s = 0{\cdot}2$ the overall Sherwood number is below 2 for both spheres at a Peclét number of $1{\cdot}0$. Looking only at sphere B the overall Sherwood number drops below 2 at a spacing of $z_s = 1{\cdot}0$ at a Peclét number of 5 and at a spacing of $z_s = 0{\cdot}2$ at a Peclét number as high as 10! Cornish [6] has reported the theoretical values of the Sherwood number for two spheres in the limiting case of zero Peclét number (mass transfer by molecular diffusion only). Using a very large value for the outer boundary ($R_\infty = 40$) we have computed Sherwood numbers for the limiting case of zero Peclét number by setting the velocities V_θ^* and V_z^* equal to zero. The results obtained from the numerical computations are compared with the theoretical values in the table below:

Sphere spacing		*Numerical results*		*Theoretical*	*Tolerance*
z_s	L/R	*Sphere A*	*Sphere B*	*values*	
0·2	2·0402	1·39239	1·39231	1·3920	10^{-6}
1·0	3·0862	1·54658	1·54653	1·5232	10^{-6}
2·1	8·288	1·80739	1·80693	1·7852	10^{-5}
3·0	20·14	1·92645	1·92597	1·9056	10^{-5}

As can be seen from the table the numerical results show excellent agreement with the theoretical values and show without question that the overall Sherwood number around a sphere in a two sphere system by molecular diffusion alone is always less than that around a single isolated sphere. This is very similar to the well known experimental observation that the drag on a sphere in a two sphere system settling one on top of the other in an unbounded fluid in Stokes' flow is always less than that of a single isolated sphere settling alone. The fact that the numerical results are so close to the theoretical values also lends further credence to the accuracy of the numerical results at the higher Peclét numbers where no analytical solutions, and limited experimental data are available for mass transfer from a two sphere system.

CONCLUDING REMARKS

Numerical solutions of the mass-transfer rates around two equally sized spheres placed parallel to their line of centers in Stokes' flow have been obtained for four different sphere spacings in the Peclét number range of 0–50. The overall Sherwood number for either sphere was always less than that of a single isolated sphere and at low Peclét numbers, overall Sherwood numbers of less than 2 were obtained. Thus the effect of particle-to-particle interaction on the mass-transfer process is significant and may be the cause for some of the very low experimental particle-to-fluid Sherwood or Nusselt number data reported for fluidized beds at low Peclét numbers.

REFERENCES

1. V. G. Levich, *Physicochemical Hydrodynamics*. Prentice-Hall, Englewood Cliffs (1962).
2. S. K. Friedlander, A note on transport to spheres in Stokes' flow, *A.I.Ch.E. Jl* **7**, 347 (1961).
3. A. C. Lochiel and P. H. Calderbank, Mass transfer in the continuous phase around axisymmetric bodies of revolution, *Chem. Engng Sci.* **19**, 471 (1964).
4. R. Pfeffer, Heat and mass transport in multiparticle systems, *I/EC Fundamentals* **3**, 380 (1964).
5. R. Pfeffer and J. Happel, An analytical study of heat and mass transfer in multiparticle systems at low Reynolds number, *A.I.Ch.E. Jl* **10**, 605 (1964).
6. A. R. H. Cornish, Note on minimum possible rate of heat transfer from a sphere when other spheres are adjacent to it, *Trans. Instn Chem. Engrs* **43**, 332 (1965).
7. M. Stimson and G. B. Jeffery, The motion of two spheres in a viscous flow, *Proc. R. Soc.* **A111**, 110 (1926).
8. T. R. Al Taha, A numerical solution of Navier–Stokes and energy equations for heat transfer from particles, Ph.D. Thesis, Imperial College, University of London (1969).

9. K. Aminzadeh, Mass and heat transfer from two spheres in creeping flow, M.Sc. Thesis, Imperial College, University of London (1970).
10. W. C. Chen and R. Pfeffer, Local and overall mass transfer rates around solid spheres with first order homogeneous chemical reaction, *I/EC Fundamentals* **9**, 101 (1970).
11. T. Yuge, Theory of heat transfer of spheres in uniform stream at low Reynolds numbers, *Rept. Inst. High Sp. Mech., Tokoku Univ.* **6**, 143 (1956).
12. A. Peltzman and R. Pfeffer, Mass transfer rates with first-order homogeneous chemical reaction around two spheres, *Chem. Engng Prog. Symp. Ser.* **63**, 49 (1967).
13. W. C. Chen and R. Pfeffer, Mass transfer rates with first-order homogeneous chemical reaction around two spheres, *Chem. Engng Prog. Symp. Ser.* **66**, 109 (1970).

APPENDIX

Development of the Finite Difference Approximations

In Fig. 3 the dimensionless concentration at points 1, 2, 3, 4 can be expressed by use of Taylor series expansion in terms of the concentration at the central point A.

$$C^*_{i+1,j} = C^*_{i,j} + h\frac{\partial C^*_{i,j}}{\partial z} + \frac{h^2}{2!}\frac{\partial^2 C^*_{i,j}}{\partial z^2} \tag{A1a}$$

$$C^*_{i-1,j} = C^*_{i,j} - h\frac{\partial C^*_{i,j}}{\partial z} + \frac{h^2}{2!}\frac{\partial^2 C^*_{i,j}}{\partial z^2} \tag{A1b}$$

$$C^*_{i,j+1} = C^*_{i,j} + k\frac{\partial C^*_{i,j}}{\partial \theta} + \frac{k^2}{2!}\frac{\partial^2 C^*_{i,j}}{\partial \theta^2} \tag{A2a}$$

$$C^*_{i,j-1} = C^*_{i,j} - k\frac{\partial C^*_{i,j}}{\partial \theta} + \frac{k^2}{2!}\frac{\partial^2 C^*_{i,j}}{\partial \theta^2}. \tag{A2b}$$

By elimination, approximate expressions for the partial derivatives at point (ih, jk) can be found in terms of the five point values of the concentration.

$$\frac{\partial C^*_{i,j}}{\partial z} = (C^*_{i+1,j} - C^*_{i-1,j})/2h \tag{A3}$$

$$\frac{\partial C^*_{i,j}}{\partial \theta} = (C^*_{i,j+1} - C^*_{i,j-1})/2k \tag{A4}$$

$$\frac{\partial^2 C^*_{i,j}}{\partial z^2} = (C^*_{i+1,j} - 2C^*_{i,j} + C^*_{i-1,j})/h^2 \tag{A5}$$

$$\frac{\partial^2 C^*_{i,j}}{\partial \theta^2} = (C^*_{i,j+1} - 2C^*_{i,j} + C^*_{i,j-1})/k^2. \tag{A6}$$

Equation (18) (see text) can also be written as:

$$\frac{\partial^2 C^*}{\partial z^2} + \frac{\partial^2 C^*}{\partial \theta^2} - \frac{\sinh z}{\cosh z - \cos\theta}\frac{\partial C^*}{\partial z} + \frac{(\cos\theta\cosh z) - 1}{\sin\theta(\cosh z - \cos\theta)}\frac{\partial C^*}{\partial \theta} = \tfrac{1}{2}N_{Pe}\frac{a^*}{\cosh z - \cos\theta}\left(V_z^*\frac{\partial C^*}{\partial z} + V_\theta^*\frac{\partial C^*}{\partial \theta}\right). \tag{18a}$$

By substituting equations (A3) to (A6) into equation (18a) we obtain the finite difference equation below:

$$C^*_{i,j} = B_1(i,j)C^*_{i+1,j} + B_2(i,j)C^*_{i-1,j} + B_3(i,j)C^*_{i,j+1} + B_4(i,j)C^*_{i,j-1} \tag{A7}$$

which is also given as equation (19), in the text, where

$$B_1(i,j) = \frac{\left[\frac{1}{h^2} - \frac{\sinh z}{2h(\cosh z - \cos\theta)} - \frac{N_{Pe}a^*V_z^*}{4h(\cosh z - \cos\theta)}\right]}{\left(\frac{2}{h^2} + \frac{2}{k^2}\right)} \tag{A8}$$

$$B_2(i,j) = \frac{\left[\frac{1}{h^2} + \frac{\sinh z}{2h(\cosh z - \cos\theta)} + \frac{N_{Pe}a^*V_z^*}{4h(\cosh z - \cos\theta)}\right]}{\left(\frac{2}{h^2} + \frac{2}{k^2}\right)} \tag{A9}$$

$$B_3(i,j) = \frac{\left[\frac{1}{k^2} + \frac{\cos\theta\cosh z - 1}{2k\sin\theta(\cosh z - \cos\theta)} - \frac{N_{Pe}a^*V_\theta^*}{4k(\cosh z - \cos\theta)}\right]}{\left(\frac{2}{h^2} + \frac{2}{k^2}\right)} \tag{A10}$$

$$B_4(i,j) = \frac{\left[\frac{1}{k^2} - \frac{\cos\theta\cosh z - 1}{2k\sin\theta(\cosh z - \cos\theta)} + \frac{N_{Pe}a^*V_\theta^*}{4k(\cosh z - \cos\theta)}\right]}{\left(\frac{2}{h^2} + \frac{2}{k^2}\right)}. \tag{A11}$$

Along the axis of symmetry we have to satisfy the condition outside the two spheres, i.e.

$$\text{at} \quad \theta = 0, \qquad \frac{\partial C^*}{\partial \theta} = 0$$

and between the two spheres,

$$\text{at} \quad \theta = \pi, \qquad \frac{\partial C^*}{\partial \theta} = 0.$$

As can be seen from equation (18a) special treatment is required because, although $\partial C^*/\partial\theta = 0$ at $\theta = 0$, $\sin\theta$ also equals zero. Therefore, a limiting process is used to determine the requisite values.

$$\operatorname*{Limit}_{\theta\to 0}\frac{\cos\theta\cosh z - 1}{\sin\theta(\cosh z - \cos\theta)}\frac{\partial C^*}{\partial \theta} = \frac{\partial^2 C^*}{\partial \theta^2}.$$

With the inclusion of $V_\theta = 0$ at $\theta = 0$ equation (18a) becomes:

$$\frac{\partial^2 C^*}{\partial z^2} + 2\frac{\partial^2 C^*}{\partial \theta^2} - \frac{\sinh z}{\cosh z - 1}\frac{\partial C^*}{\partial z} = \tfrac{1}{2}N_{Pe}\frac{a^*V_z^*}{\cosh z - 1}\frac{\partial C^*}{\partial z}. \tag{18b}$$

By similar reasoning, for $\theta = \pi$ equation (18a) becomes

$$\frac{\partial^2 C^*}{\partial z^2} + 2\frac{\partial^2 C^*}{\partial \theta^2} - \frac{\sinh z}{\cosh z + 1}\frac{\partial C^*}{\partial z} = \tfrac{1}{2}N_{Pe}\frac{V_z^*}{\cosh z + 1}\frac{\partial C^*}{\partial z}. \tag{18c}$$

Obviously these equations (18b) and (18c) require special treatment because in order to expand them at $\theta = 0$ and $\theta = \pi$ only three points are available (see Fig. 3, point B).

Therefore, the equations for the derivatives are given as:

along $\theta = 0$ $(j = 1)$

$$\frac{\partial C^*_{i,1}}{\partial z} = (C^*_{i+1,1} - C^*_{i-1,1})/2h \tag{A12}$$

$$\frac{\partial^2 C^*_{i,1}}{\partial z^2} = (C^*_{i+1,1} - 2C^*_{i,1} + C^*_{i-1,1})/h^2 \tag{A13}$$

along $\theta = \pi$ $(j = m1)$

$$\frac{\partial C^*_{i,m1}}{\partial z} = (C^*_{i+1,m1} - C^*_{i-1,m1})/2h \tag{A14}$$

$$\frac{\partial^2 C^*_{i,m1}}{\partial z^2} = (C^*_{i+1,m1} - 2C^*_{i,m1} + C^*_{i-1,m1})/h^2. \tag{A15}$$

From equation (A3) we find for $\theta = 0$ $(j = 1)$:

$$\frac{\partial^2 C^*_{i,1}}{\partial \theta^2} = 2(C^*_{i,2} - C^*_{i,1})/k^2. \tag{A16}$$

From equation (A4) we find for $\theta = \pi$ $(j = m1)$:

$$\frac{\partial^2 C_{i,m1}}{\partial \theta^2} = 2(C^*_{i,m} - C^*_{i,m1})/k^2. \tag{A17}$$

The substitutions of equations (A12), (A13) and (A16) into equation (18a) gives the following finite difference equations at $\theta = 0$:

$$C^*_{i,1} = A_1(i)C^*_{i+1,1} + A_2(i)C^*_{i-1,1} + A_3 C^*_{i,2} \tag{A18}$$

which is also given as equation (20) in the text, where

$A_1(i)$

$$= \left[\frac{1}{h^2} - \frac{\sinh z}{2h(\cosh z - 1)} - \frac{N_{Pe}a^*V_z^*}{4h(\cosh z - 1)}\right] \Big/ \left(\frac{2}{h^2} + \frac{4}{k^2}\right) \tag{A19}$$

$A_2(i)$

$$= \left[\frac{1}{h^2} + \frac{\sinh z}{2h(\cosh z - 1)} - \frac{N_{Pe}a^*V_z^*}{4h(\cosh z - 1)}\right] \Big/ \left(\frac{2}{h^2} + \frac{4}{k^2}\right) \tag{A20}$$

$$A_3 = \frac{2}{k^2} \Big/ \left(\frac{1}{h^2} + \frac{2}{k^2}\right). \tag{A21}$$

Similarly the substitution of equations (A14), (A15) and (A17) into equation (18c) gives the following finite difference equation at $\theta = \pi$:

$$C^*_{i,m1} = D_1(i)C^*_{i+1,m1} + D_2(i)C^*_{i-1,m1} + D_3 C^*_{i,m} \tag{A22}$$

which is also given as equation (21) in the text, where

$D_1(i)$

$$= \left[\frac{1}{h^2} - \frac{\sinh z}{2h(\cosh z + 1)} - \frac{N_{Pe}a^*V_z^*}{4h(\cosh z + 1)}\right] \Big/ \left(\frac{2}{h^2} + \frac{4}{k^2}\right) \tag{A23}$$

$D_2(i)$

$$= \left[\frac{1}{h^2} + \frac{\sinh z}{2h(\cosh z + 1)} + \frac{N_{Pe}a^*V_z^*}{4h(\cosh z + 1)}\right] \Big/ \left(\frac{2}{h^2} + \frac{4}{k^2}\right) \tag{A24}$$

$$D_3 = \frac{2}{k^2} \Big/ \left(\frac{1}{h^2} + \frac{2}{k^2}\right). \tag{A25}$$

The value of V_z^* in equations (A18) and (A22) is evaluated as follows: Assume $\partial V_z^*/\partial\theta = 0$ along the axis of symmetry at $\theta = 0$ and $\theta = \pi$. Also approximate $\partial V_z^*/\partial\theta$ as a function of the values of V_z^* at the interior points using (see [8]):

$$\left.\frac{\partial V_z^*}{\partial \theta}\right|_{i,1} = \frac{1}{12h}(-25V_z^*(i,1) + 48V_z^*(i,2) - 36V_z^*(i,3) + 16V_z^*(i,4) - 3V_z^*(i,5)) \tag{A26}$$

which gives at $\theta = 0$

$$V_z^*(i,1) = 1{\cdot}92V_z^*(i,2) - 1{\cdot}44V_z^*(i,3) + 0{\cdot}64V_z^*(i,4) - 0{\cdot}12V_z^*(i,5). \tag{A27}$$

Similarly along $\theta = \pi$

$$V_z^*(i,m1) = 1{\cdot}92V_z^*(i,m) - 1{\cdot}44V_z^*(i,m-1) + 0{\cdot}64V_z^*(i,m-2) - 0{\cdot}12V_z^*(i,m-3). \tag{A28}$$

TRANSPORT MASSIQUE AUTOUR DE DEUX SPHERES A FAIBLE NOMBRE DE REYNOLDS

Résumé—On a utilisé une technique de relaxation pour résoudre l'équation de conservation des espèces et obtenir les flux de transfert massique autour de deux sphères identiques, avec la ligne des centres parallèle à un écoulement de Stokes. On considère quatre espacements différents dans un domaine de nombre de Péclet allant de zéro à 50. On trouve que le nombre de Sherwood pour chaque sphère est toujours inférieur à celui d'une sphère unique, et on obtient aux faibles nombres de Péclet des nombres globaux de Sherwood inférieurs à 2.

STOFFTRANSPORT AUS ZWEI KUGELN BEI NIEDRIGEN REYNOLDS-ZAHLEN

Zusammenfassung—Eine Relaxationsmethode wurde dazu benutzt, die speziellen Erhaltungssätze zu lösen, aus denen man die übergehenden Stoffmengen aus zwei Kugeln gleichen Durchmessers erhält, die parallel zu ihrer Mittelachse in einer Stokes' schen Strömung angeordnet sind. Vier verschiedene Kugelabstände wurden im Bereich der Péclet-Zahlen von 0 bis 50 untersucht. Dabei zeigte sich, daß die mittleren Sherwood-Zahlen für beide Kugeln immer kleiner waren als die einer einzelnen Kugel. Bei niedrigen Péclet-Zahlen wurden mittlere Sherwood-Zahlen unter 2 erhalten.

МАССООБМЕН ДВУХ СФЕР ПРИ НИЗКИХ ЧИСЛАХ РЕЙНОЛЬДСА

Аннотация — Используется релаксационный метод решения уравнения сохранения вещества для определения интенсивности массообмена в стоксовском потоке двух сфер одинакового размера, помещенных параллельно линии их центров. Исследовались четыре различных расстояния между сферами в диапазоне чисел Пекле от 0 до 50. Найдено, что общее число Шервуда для любой из сфер всегда меньше, чем это же число для одной изолированной сферы. Для низких чисел Пекле получены общие числа Шервуда меньше 2.